Vacuum 211 (2023) 111952

Contents lists available at ScienceDirect

Vacuum

journal homepage: www.elsevier.com/locate/vacuum

# Atomistic simulations of defect clustering evolution in heavily irradiated Ti35 alloy

Hai Huang [a,b,*], Longjingrui Ma [a], Tianci Liu [a], Bin Cai [a,b], Huan Li [c], Qing Peng [d]

[a] Key Laboratory of Material Physics of Ministry of Education, School of Physics and Microelectronics, Zhengzhou University, Zhengzhou, 450052, China
[b] Institute of Intelligent Sensing, Zhengzhou University, Zhengzhou, 450001, China
[c] Xi'an Rare Metal Materials Institute Co.Ltd, Xi'an, 710016, China
[d] State Key Laboratory of Nonlinear Mechanics, Institute of Mechanics, Chinese Academy of Sciences, Beijing, 100190, China

ARTICLE INFO

Handling Editor: Luigia Sabbatini

*Keywords:*
Ti35 alloy
Heavy irradiation damage
Frenkel pair accumulation
Defect clustering
Tantalum enrichment
Molecular dynamics

ABSTRACT

Ti35 alloy (Ti-6wt.%Ta) has greatly promising applications in nuclear industries due to its excellent overall performance. Nevertheless, atomistic mechanisms of its defect clustering evolution due to long-term exposure to irradiation remain scarcely understood by far. Here we investigate the heavy irradiation damage in Ti35 alloy with a dose of up to 4.0 canonical displacement per atom (cDPA) using atomistic simulations of Frenkel pair accumulation. Results show that defect clustering becomes remarkable before 0.04 cDPA and thereafter tends to be relatively stable, and the fraction is not directly dependent on the irradiation dose. Interstitials exhibit a stronger ability than vacancies to form clusters and especially the $N_{int}$>5 clusters may cause the formation of 1/3<1$\bar{1}$210> dislocation loops. Compared to the matrix, $N_{int}\leq$5 interstitial-type defects show a depletion of Ta atoms, while $N_{int}$>5 clusters are Ta-rich. This study provides an important insight into the understanding of the irradiation damage behaviors for Ti35 alloy.

Titanium (Ti) alloys, because of their superior mechanical properties, corrosion resistance, and low neutron-induced activity, have attracted tremendous attention in the nuclear industries in recent decades [1–6]. Among the variety of Ti-based materials, the α-type Ti35 alloy (Ti-6wt.% Ta) has been proven to possess excellent long-term corrosion resistance in a nitric acid solution containing fluoride ions (akin to the corrosive environment of the next-generation molten salt reactors [7]) and successfully applied in a spent nuclear fuel reprocessing facility in China [8–11]. On the other hand, motivated by the demand for developing new materials for advanced nuclear reactors, it has also been highly expected to adopt Ti35 alloy as the in-core structural material [9]. In these nuclear applications, one problem for the Ti35 alloy that has to be faced is serious irradiation damage [1–6]. Nevertheless, to the best of our knowledge, current research on Ti35 alloy has focused on examining its corrosive and mechanical characteristics, and the irradiation effects of Ti35 alloy have rarely been studied [12], especially the physical reasoning behind the defect clustering evolution on the atomic scale due to long-term irradiation. Therefore, understanding the irradiation damage behaviors early is of fundamental importance for developing irradiation-resistant Ti35 alloy for nuclear applications.

From the present reality perspective, classical molecular dynamics (MD) is still the most appropriate method to study the mobility of defects, clustering evolution, and their interactions, compared to experimental measurements with various limitations [13–16]. In particular, the Frenkel pair accumulation (FPA) method based on MD technology, proposed by Christensen et al. [17] and Derlet et al. [18], provides a feasible path for simulating a material irradiated to a dose as high as several displacements per atom (DPA). In this method, randomly distributed Frenkel pairs (FPs) produced by a displacement cascade are artificially inserted into their matrix periodically, followed by static and thermodynamic relaxations between adjacent insertions, in which we can observe long-term irradiation-induced damage. For example, Maxwell et al. [19] reasonably stated the mechanisms of experimentally observed anisotropic growth of Zr based on the method. Hence, the FPA method is adopted herein to investigate the defect clustering evolution in an irradiated Ti35 alloy, and the effect of Ta on defect clustering is focused on.

FPA simulations were implemented based on the parallel MD code LAMMPS [20], and subsequent visualizations were rendered with

* Corresponding author. Key Laboratory of Material Physics of Ministry of Education, School of Physics and Microelectronics, Zhengzhou University, Zhengzhou, 450052, China.
*E-mail address:* huanghai@zzu.edu.cn (H. Huang).

https://doi.org/10.1016/j.vacuum.2023.111952
Received 19 November 2022; Received in revised form 24 February 2023; Accepted 24 February 2023
Available online 26 February 2023

OVITO software [21]. For the simulations, a single crystal hcp-Ti35 cubic box with the size of 73.7 × 102.1 × 120.3 Å$^3$ (containing 50, 000 atoms ($N_{total}$)) was created along [$\bar{1}$2$\bar{1}$0], [$\bar{1}$010], and [0001] crystallographic orientations, in which 830 Ta atoms, corresponding to a concentration of 1.7 at.%, are randomly distributed. The Ti–Ti, Ti–Ta, and Ta–Ta interactions were described by the embedded atom method (EAM) potential developed by Zhou et al. [22]. Each calculation was run by imposing periodic boundary conditions. After a conjugate gradient (CG) minimization, the single crystal was thermally relaxed with the Nose-Hoover isobaric-isothermal ensemble (NPT) under zero pressure at 300 K for 20 ps. Subsequently, the FPA procedure was initiated as follows: 1) $N_{def}$ atoms were randomly chosen and removed, and then the same number of atoms were inserted at different random sites in the system; 2) Then the damaged system was subjected to a CG minimization to release the stress (*i.e.*, iteratively adjusting atom coordinates and pushing the highly overlapped atoms (large energies and forces) off of each other) and then re-equilibrated with NVT ensemble at 300 K; 3) Steps 1) and 2) were repeated until reaching the desired irradiation dose. Herein, the $N_{def}$ was determined as 20 in each loop, corresponding to an increment of 4 × 10$^{-4}$ canonical DPA (cDPA, a DPA literal meaning defined in Ref. [18]). The relaxation time of each loop varied from 67.5 to 562.5 ps with a time step of 0.005 ps. Eventually, the irradiation dose of 4.0 cDPA (*i.e.*, 10,000 × $N_{def}/N_{total}$) was received by executing 10,000 loops, and the average dose rate was regulated as 5.525 × 10$^6$ cDPA·s$^{-1}$, the same order of magnitude as the previous studies [19,23]. The Wigner–Seitz cell method [16,23] was employed to detect the FPs during irradiation, and the cluster analysis with a cutoff radius of 3.1 Å (*i.e.*, 0.2 Å larger than the distance of nearest-neighbor atoms predicted by the EAM potential [22]) was further applied to identify defect clusters.

Fig. 1 displays the snapshots of the defect distributions in the simulation box after 0.04, 0.173, 2.0, and 4.0 cDPA, respectively. These

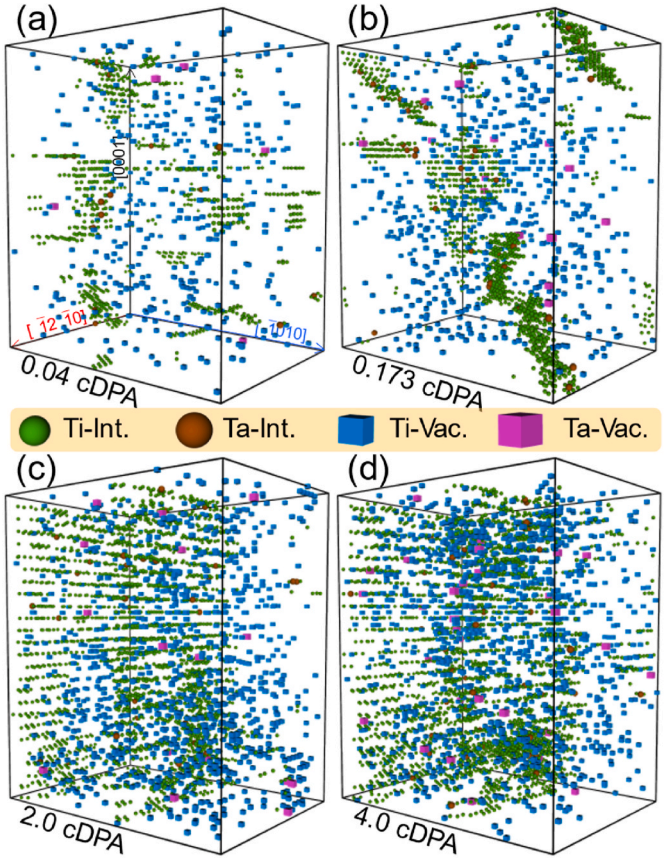


**Fig. 1.** Defect distributions obtained after different irradiation doses in the simulation box. (**a**) 0.04 cDPA. (**b**) 0.173 cDPA. (**c**) 2.0 cDPA. (**d**) 4.0 cDPA.

four doses are selected because they correspond to the ascent, vicinity of initial saturation site, dose midpoint, and final state in the profile of the surviving FPs related to irradiation dose in the system [18,24], respectively, which facilitates vivid clarification of the defect evolution. At the dose of 0.04 cDPA, very few vacancies form clusters because they have been away from each other, while most of the interstitials show significant clustering. This may be because the migration energy of interstitials is usually significantly lower than that of vacancies [25,26], which causes a rapid migration and aggregation of interstitials while a relative difficulty for vacancies to migrate at 300 K within the MD time scale. After 0.173 cDPA, small vacancy clusters show an increase, while interstitial clustering behavior further intensifies and causes the continuous aggregation of dispersed small clusters into large clusters. Especially, most of the large interstitial clusters seem to prefer to arrange along the *xz*-crystallographic plane and adsorb several Ta atoms. At 2.0 cDPA, a very noticeable phenomenon is that most of the interstitials are further clustered and zonally distributed on the same crystallographic planes, which may be due to the formation of interstitial-type dislocation that is like the observation in hcp-Zr by Maxwell et al. [19]. The large interstitial clusters always remain in the plane configuration before reaching 4.0 cDPA, highlighting the stabilization of the defect configuration. Despite a significant increase in dose, the vacancies are still scattered all over the box and only form small clusters rather than large clusters (see Fig. 1(d)), like the situation at 0.173 cDPA. These suggest that the continued increase in dose after 2.0 cDPA does not result in a fundamental change in the distribution of defects but only induces the reorganization of local crystal defects. During the whole process, more and more Ta atoms are displaced from their lattice sites and captured into interstitial clusters, which may play a role in pinning the clusters and suppressing their growth [27].

The clustering fractions related to the cluster size at different doses are shown in Fig. 2 to highlight the defect clustering behaviors. The clustering fraction of interstitials or vacancies at a certain irradiation dose is counted according to the following equation [28].

$$\sigma_X = \frac{\sum_{i=0}^{n} N_X^i}{N_{FPs}} \tag{1}$$

where $N_X^i$ denotes the number of X (*i.e.*, interstitial or vacancy) in the *i*th X cluster, and *n* represents the total number of X clusters. When $N_{vac} \geq 3$ or $N_{int} \geq 4$, it is simply identified as a vacancy or interstitial cluster, respectively [28]. Both interstitials and vacancies show a fast-clustering rate before 0.04 cDPA and thereafter seem to have a relatively stable clustering. For the case of interstitial clustering, an almost constant proportion of zero occurs for the $N_{int} = 5$ clusters over the course of the process, while the proportions of $N_{int} = 4$ and $N_{int} > 5$ clusters mainly fluctuate around 10% and 80%, respectively, independent of irradiation doses. In addition, the proportion of interstitials not in any clusters only accounts for approximately 10% on most occasions. These indicate that it is easy for interstitials to aggregate after irradiation. Noticeably, the proportions between different types of interstitial clusters seem to exhibit the behavior of transformation periodically during irradiation, which is mainly manifested as an increase or decrease in the reverse of the proportions of low-order (*e.g.*, $N_{int} = 4$ or $N_{int} < 4$) and high-order (*i.e.*, $N_{int} > 5$) clusters, shown along the guidance arrows in Fig. 2(a). This reverse behavior may be explained simply as follows. On one hand, since the low-order clusters are often prone to become the nucleation sites of prism-plane dislocation loops in hcp crystals that give them relatively low formation energy [29,30], they tend to glide back and forth along the [$\bar{1}$2$\bar{1}$0] direction and then aggregate quickly or be trapped by other large clusters, causing a decline in the proportion of low-order clusters while an increase in the proportion of high-order clusters. On the other hand, a supersaturated large cluster may be decomposed into several small clusters (*e.g.*, $N_{int} = 4$ clusters) or isolated interstitials under local deformation stress during its migration, which can again

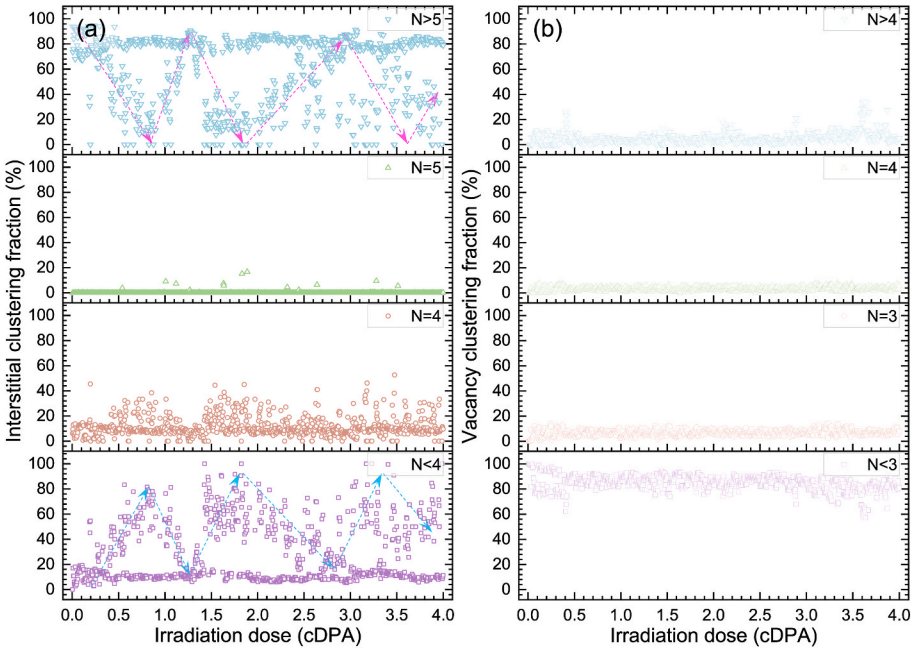


**Fig. 2.** Fractions of point defects in clusters of different sizes as a function of dose. (**a**) Interstitial. (**b**) Vacancy. Transformation periodically in $N_{int} < 4$ or $N_{int} > 5$ clusters is marked out by dotted arrows.

cause the increase of the proportion of low-order clusters while the decrease of the proportion of high-order clusters. For the case of vacancy clustering, the proportions of $N_{vac} = 3$, $N_{vac} = 4$, and $N_{vac} > 4$ clusters, from an overall perspective, almost remain stable around 8%, 4%, and 4%, respectively, all of which are far below that (approximately 84%) of vacancies not in any clusters. The very low proportion of vacancy clusters (especially $N_{vac} > 3$ clusters) indicates that the formation of large clusters is very difficult in this study due to the high migration energy of vacancies at 300 K [27,30] and a lack of quick defect annealing like that during collision cascades [16,25]. Consequently, this makes the vacancies not in any clusters have the highest proportion, which may have an important impact on vacancy clustering and evolution at high doses. A combination of the FPA algorithm and collision cascade simulations may be required to further clarify it in the future work. Taken together, the clustering fraction of interstitials is significantly higher than that of vacancies. Interstitials have a greater probability of forming large clusters, while it is very difficult for vacancies to accumulate into voids under current conditions. Many experimental observations have demonstrated that the failure of metals is dominated by irradiation hardening and embrittlement below $0.4T_m$ (where $T_m$ denotes the melting temperature) [31], which results from the generation of interstitial-type dislocations or dislocation loops and their interactions [32,33]. The phenomenon observed in this work that the interstitial-type dislocations are more prone to form can also confirm the experimental conclusions. In addition, in a sense, an increase in irradiation dose does not seem to trigger irregular changes in the proportions of different types of interstitial or vacancy clusters.

To acquire a better intuition of the evolution of different types of clusters, the snapshots of the distributions of interstitial and vacancy clusters with different sizes in the simulation box after 0.04, 0.173, 2.0, and 4.0 cDPA are presented in Fig. 3 and A1, respectively. At 0.04 cDPA, only four $N_{int} = 4$ clusters form, even inexistent for $N_{int} = 5$ clusters, while most of the interstitials aggregate into $N_{int} > 5$ clusters, which are distributed in various areas of the box. Several complex interstitial clusters have emerged. A handful of interstitials not in any clusters are retained, whereas most of the vacancies don't cluster, highlighting that interstitials are more likely to form clusters (especially $N_{int} > 5$ clusters) than vacancies at 300 K. At 0.173 cDPA, the $N_{int} > 5$ clusters exhibit a decline in number density while an increase in size, which may be attributed to the aggregation between clusters and their capture of surrounding interstitials. Apart from $N_{int} > 5$ clusters, there is no significant change for other interstitial clusters. We can observe that most of the $N_{int} > 5$ clusters have the same arrangement as that of parallel crowdions with their axis along the $[\bar{1}2\bar{1}0]$ direction, and the complex clusters tend to form the dislocation loops with a Burgers vector of $\boldsymbol{b} = 1/3\langle 1\bar{2}10\rangle$ as this type of dislocation is energetically favorable in hcp crystals. Meanwhile, vacancies in number and their clustering are increased, but the number of clusters is still relatively low. At 2.0 cDPA, either interstitials or vacancies, their low-order clusters increase in number, and the high-order clusters have a significant enlargement in size. Further analysis reveals that the region around the flat and large clusters in Fig. 3(c4) mainly generates a $1/3\langle 1\bar{2}10\rangle$ interstitial-type dislocations loop (with a length of 134.7 Å) aligned in bands parallel with the $(\bar{1}010)$ plane due to the continuous glide and aggregation of low-order clusters along the $[\bar{1}2\bar{1}0]$ direction, highly consistent with the experimental observations in other Ti alloys [2]. Especially, the dislocations could trap their nearby defects and then keep growing at higher doses. The emergence of an extra interstitial plane near the cell boundary also may be because the growth of a dislocation penetrates the boundary and it feels own forces. Further studies may need to clarify this point. At 4.0 cDPA, apart from the further growth of the flat interstitial-type defects in Fig. 3(d4), other interstitial clusters have no noteworthy difference in number and size relative to those at 2.0 cDPA, suggesting that the scale of interstitial clustering has already been close to its saturation. Furthermore, there is still a continuous increase in the number of vacancy clusters, as well as their sizes, because of the further trapping of clusters on nearby vacancies. This indicates that vacancy clustering has not reached its saturation point after irradiation of 4.0 cDPA dose.

In Fig. 3, the distributions of Ta atoms in different interstitial clusters also can be observed. With the increase of irradiation dose, the number of Ta atoms in clusters, especially in $N_{int} > 5$ clusters, has a slightly increasing trend. However, compared to Ti atoms, the content of Ta atoms in the clusters appears to be much lower. In addition, the segregation of Ta also does not occur in the clusters. To further understand the effect of Ta on clustering, the fractions of Ta atoms in interstitial clusters of different sizes versus irradiation doses are shown in Fig. 4. The Ta concentration in interstitial clusters at a certain irradiation dose can be

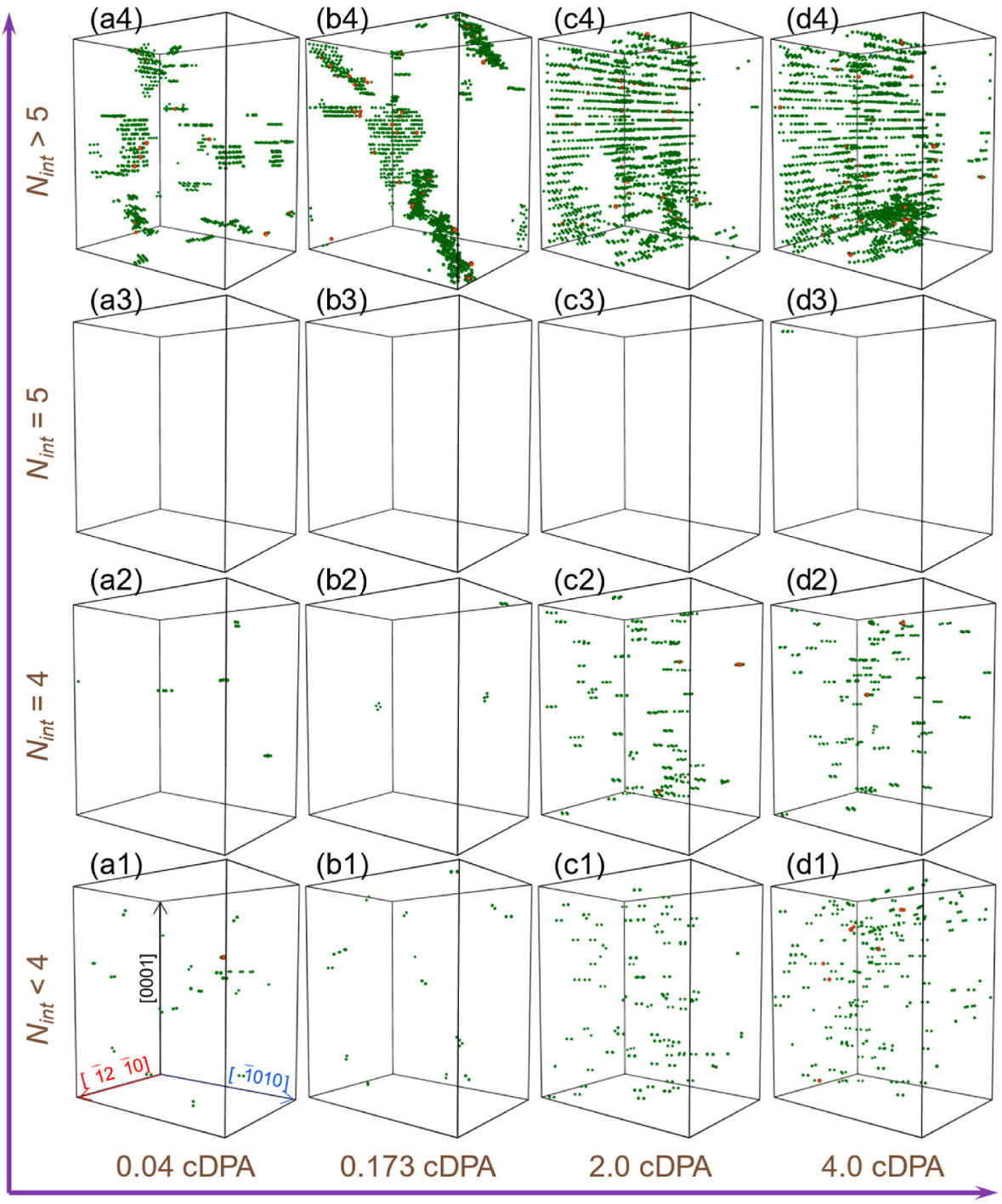


**Fig. 3.** Distributions of interstitial clusters of different sizes after different irradiation doses in the simulation box. (**a**) 0.04 cDPA. (**b**) 0.173 cDPA. (**c**) 2.0 cDPA. (**d**) 4.0 cDPA.

obtained as follows

$$\sigma_{Ta} = \frac{\sum_{i=0}^{n} \left(N_{Ta} \middle| N_{int}^{i}\right)}{\sum_{i=0}^{n} N_{int}^{i}} \tag{2}$$

where $N_{int}^{i}$ refers to the number of interstitials in the $i$th cluster, and $N_{Ta}|N_{int}^{i}$ is the number of Ta atoms in the $i$th cluster. Like that in Fig. 2(a), the fraction of Ta atoms presents a rapid increase before 0.2 cDPA, and thereafter tends to stabilize in the form of fluctuations. After 0.2 cDPA, the fractions of Ta atoms in $N_{int} = 4$ and $N_{int} > 5$ clusters mainly fluctuate around 0.5% and 4.5%, respectively, and approximately 0.5% of Ta defects not in any clusters. Due to almost no $N_{int} = 5$ clusters, the fraction of Ta atoms in such clusters remains zero. Compared to the Ta concentration of raw alloy, the $N_{int} \leq 5$ interstitial-type defects show a depletion of Ta almost throughout the irradiation process, while the $N_{int} > 5$ clusters are Ta-rich. Granberg et al. [27] investigated the response of several FeCr alloys with different Cr contents (varying from 2.5 to 20 at. %) to massively overlapping cascades and found that different from the medium (only Cr-rich in single interstitials) and high (Cr-depleted in all sizes of interstitial clusters) Cr-containing alloys, not only low-order clusters but high-order clusters have an excess of Cr in the low

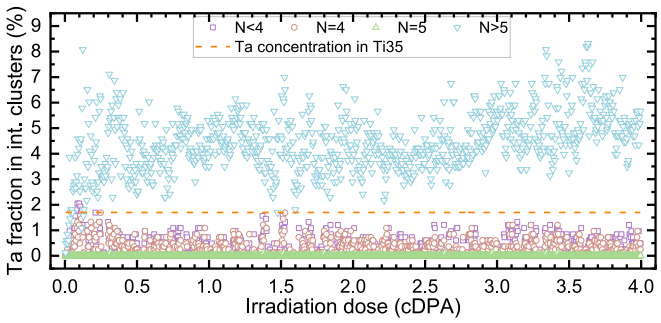


**Fig. 4.** Fractions of Ta atoms in interstitial clusters of different sizes. The dashed line denotes the Ta concentration in the raw Ti35 alloy.

Cr-containing (≤5 at.%) alloys. Considering that Ti35 alloy also has the characteristic of low solute content, the difference in Ta concentration between interstitial clusters of different sizes may be explained by referring to the low Cr-containing (≤5 at.%) alloys irradiated [27]. For the depletion of Ta in low-order clusters, this may be because, in the clusters, the average binding energy of Ti–Ti is higher than that of Ti–Ta and Ta–Ta (the highest for Fe–Cr in the low Cr-containing alloys in the same situation [27]), which makes the clustering almost completely dominated by Ti interstitials. The excess of Ta in high-order clusters could be caused by a dislocation among them (see Fig. 3(d4)). As the dislocations are usually mobile [27,32,34], they can constantly capture nearby Ta atoms during their movement and thus may have a higher Ta concentration than that of the raw alloy.

In summary, the FPA simulations based on the MD method were performed to study the defect clustering evolution in the Ti35 alloy exposure to an irradiation dose of 4.0 cDPA. Both interstitials and vacancies show a fast-clustering rate before 0.04 cDPA, and thereafter the clustering, especially for vacancies, tends to be relatively stable. The $N_{int} > 5$ clusters have the largest proportion of interstitials, reaching approximately 80% on most occasions. Only a proportion of approximately 10% belongs to the interstitials not in any clusters. In contrast, the vacancies not in any clusters have a proportion of approximately 84%, far beyond that of all vacancy clusters. This highlights that interstitials are more likely to form clusters (especially $N_{int} > 5$ clusters) than vacancies at 300 K. Generally, the $N_{int} > 5$ clusters prefer to arrange along [$\bar{1}2\bar{1}0$] direction and some complex clusters among them even evolve into the 1/3<$1\bar{2}10$> dislocation loops, particularly pronounced after 2.0 cDPA. At 4.0 cDPA, the scale of interstitial clustering has already approached saturation, while vacancy clustering is still on its way. In addition, the fractions of Ta atoms in interstitial clusters of different sizes show a stabilization in the form of fluctuations after 0.2 cDPA. Compared to the raw alloy, the $N_{int} \leq 5$ interstitial-type defects show a depletion of Ta (approximately 1.0% in total) almost throughout the irradiation process, while the $N_{int} > 5$ clusters are Ta-rich (approximately 4.5%), attributed to the high binding energy of Ti–Ti and the mobile dislocations of capturing Ta respectively. More research is still needed for complete understanding of the irradiation damage behaviors for the alloy in the future. All these results can provide a reliable theoretical basis and reference for the assessment of the irradiation tolerance of Ti35 alloy in nuclear applications.

## CRediT authorship contribution statement

**Hai Huang:** Writing – review & editing, Writing – original draft, Supervision, Methodology, Investigation, Funding acquisition, Conceptualization. **Longjingrui Ma:** Visualization, Software, Methodology, Investigation, Funding acquisition. **Tianci Liu:** Visualization, Methodology, Investigation. **Bin Cai:** Validation, Methodology, Formal analysis, Data curation. **Huan Li:** Validation, Methodology, Investigation, Conceptualization. **Qing Peng:** Writing – review & editing, Visualization, Software, Methodology, Investigation.

## Declaration of competing interest

The authors declare that they have no known competing financial interests or personal relationships that could have appeared to influence the work reported in this paper.

## Data availability

Data will be made available on request.

## Acknowledgments

This work was supported by the National Natural Science Foundation of China (Grant No. 12105249), the Key Project for Science and Technology Development of Henan Province (Grant No. 212102210195), the Innovation Team Support Program for Cooperation of Young Talents & Enterprises in Zhengzhou University (Grant No. 32320368), the Henan Province Postdoctoral Science Foundation (Grant No. 202102012), the Research and Practice Project of Education and Teaching Reform in Zhengzhou University (Grant No. 2022ZZUJG173), the Undergraduate Training Program for Innovation and Entrepreneurship in Zhengzhou University (Grant No. 2022cxcy362), the Large Power Material Irradiation Experimental System (LP-MIES) in Dalian University of Technology, and the National Supercomputing Center in Zhengzhou.

## Appendix A. Description of the distributions of different vacancy clusters

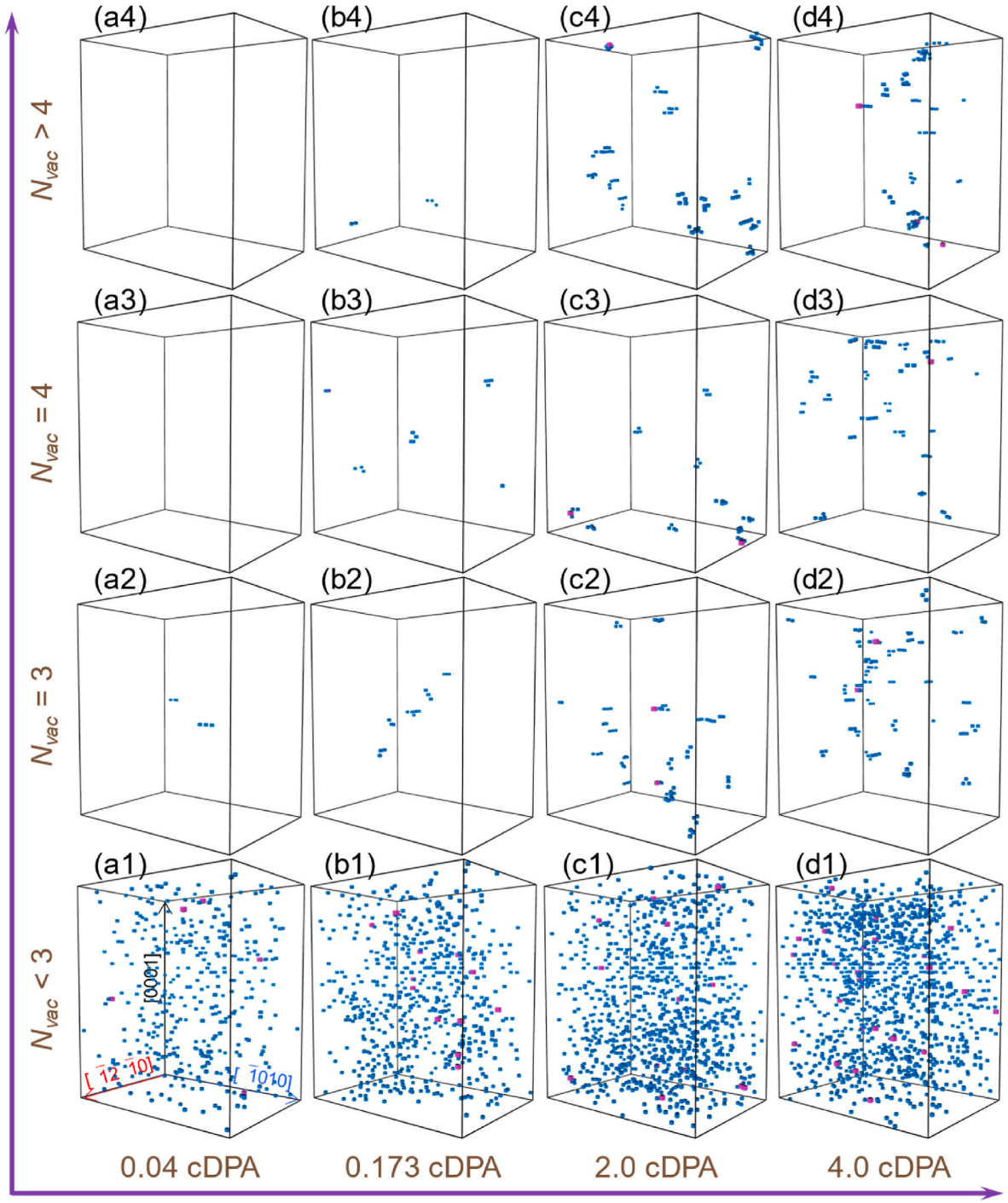


**Fig. A1.** Distributions of vacancy clusters of different sizes after different irradiation doses in the simulation box. (**a**) 0.04 cDPA. (**b**) 0.173 cDPA. (**c**) 2.0 cDPA. (**d**) 4.0 cDPA.

## References


[1] R.E. Nygren, Irradiation creep studies of titanium alloys, J. Nucl. Mater. 85 (1979) 861–865, https://doi.org/10.1016/0022-3115(79)90368-4.

[2] M. Griffiths, D. Faulkner, R.C. Styles, Neutron damage in α-titanium, J. Nucl. Mater. 119 (1983) 189–207, https://doi.org/10.1016/0022-3115(83)90196-4.

[3] L.R. de la Vega, R. Trejo-Luna, J. Rickards, L. Baños, C. Falcony, The effects of implanting various high energy ions into Ti and Ti–6Al–4V, Surf. Coating. Technol. 196 (2005) 257–261, https://doi.org/10.1016/j.surfcoat.2004.08.096.

[4] H. Zhu, Y. Ma, T. Wei, H. Li, R. Aughterson, G. Lumpkin, The formation and Kr-ion irradiation behaviour of new microstructural features in additively manufactured titanium aluminium alloy, Addit. Manuf. 29 (2019), 100766, https://doi.org/10.1016/j.addma.2019.06.017.

[5] S. Dey, A. Dutta, P. Mukherjee, N. Gayathri, A.D. Gupta, T. KunduRoy, Characterization of ion induced damage as a function of depth in proton irradiated pure Ti and Ti–6Al–4V, J. Alloys Compd. 821 (2020), 153441, https://doi.org/10.1016/j.jallcom.2019.153441.

[6] C.R. Lear, J.G. Gigax, O. El Atwani, M.R. Chancey, H. Kim, N. Li, Y. Wang, S. J. Fensin, Effects of helium cavity size and morphology on the strength of pure titanium, Scripta Mater. 212 (2022), 114531, https://doi.org/10.1016/j.scriptamat.2022.114531.

[7] C. Liu, X. Tang, L. Cheng, B. Leng, X. Li, X. Ye, H. Huang, The characterization of corrosion layers of GH3535 and Inconel 625 alloys in molten KNO3-NaNO3 salts at 500 °C, Corrosion Sci. 204 (2022), 110406, https://doi.org/10.1016/j.corsci.2022.110406.

[8] J. Xu, C. Liu, H. Li, W. Wu, J. Wu, B. Zhao, Y. Zhang, Y. Zhao, L. Zhou, Orientation dependence of corrosion resistance of a near-alpha Ti35 alloy applied in nuclear industry, J. Nucl. Mater. 568 (2022), 153873, https://doi.org/10.1016/j.jnucmat.2022.153873.
[9] J. Xu, H. Su, D. Guo, Y. Zhao, B. Xu, L. Zhou, Electrochemical corrosion behavior of Ti35 alloy in nitric acid containing fluoride ions, Rare Met. Mater. Eng. 48 (2019) 1124–1129.
[10] J. Xu, C. Liu, J. Wu, H. Li, Y. Zhang, Y. Zhao, L. Zhou, Formation and annihilation of deformation twinning in hexagonal Ti with lamellar microstructure, J. Alloys Compd. 925 (2022), 166670, https://doi.org/10.1016/j.jallcom.2022.166670.
[11] J. Xu, C. Liu, J. Wu, Bo Qi, Y. Zhang, Y. Zhao, L. Zhou, Three-dimensional microstructure and texture evolution of Ti35 alloy applied in nuclear industry during plastic deformation at various temperatures, Mater. Sci. Eng. 819 (2021), 141508, https://doi.org/10.1016/j.msea.2021.141508.
[12] H. Li, C. Liu, J. Xu, H. Huang, J. Wu, H. Liu, X. Zhao, J. Wu, Gamma-ray irradiation behavior of a hexagonal Ti–6Ta alloy applied in spent nuclear fuel reprocessing, J. Mater. Sci. 57 (2022) 1–10, https://doi.org/10.1007/s10853-022-07889-z.
[13] K. Nordlund, F. Djurabekova, Multiscale modelling of irradiation in nanostructures, J. Comput. Electron. 13 (2014) 122–141, https://doi.org/10.1007/s10825-013-0542-z.
[14] Y. Zhang, S. Zhao, W.J. Weber, K. Nordlund, F. Granberg, F. Djurabekova, Atomic-level heterogeneity and defect dynamics in concentrated solids-olution alloys, Curr. Opin. Solid St. M. 21 (2017) 221–237, https://doi.org/10.1016/j.cossms.2017.02.002.
[15] J. Peng, S. Cui, Y. Tian, Q. Fang, J. Li, P.K. Liaw, Effects of grain boundary on irradiation-induced zero-dimensional defects in an irradiated copper, Appl. Math. Mech. 43 (2022) 233–246, https://doi.org/10.1007/s10483-022-2803-5.
[16] Y. Jin, H. Huang, Y. Zhong, X. Yuan, H. Li, D. Lou, K. Xie, Z. Liu, B. Cai, Q. Peng, Role of interface on irradiation damage of Cu−diamond composites using classical molecular dynamics simulations, Ceram. Int. 48 (2022) 16813–16824, https://doi.org/10.1016/j.ceramint.2022.02.232.
[17] M. Christensen, W. Wolf, C. Freeman, E. Wimmer, R.B. Adamson, L. Hallstadius, P. E. Cantonwine, E.V. Mader, Diffusion of point defects, nucleation of dislocation loops, and effect of hydrogen in hcp-Zr: Ab initio and classical simulations, J. Nucl. Mater. 460 (2015) 82–96, https://doi.org/10.1016/j.jnucmat.2015.02.013.
[18] P.M. Derlet, S.L. Dudarev, Microscopic structure of a heavily irradiated material, Phys. Rev. Mater. 4 (2020), 023605, https://doi.org/10.1103/PhysRevMaterials.4.023605.
[19] C. Maxwell, J. Pencer, E. Torres, Atomistic simulation study of clustering and evolution of irradiation-induced defects in zirconium, J. Nucl. Mater. 531 (2020), 151979, https://doi.org/10.1016/j.jnucmat.2019.151979.
[20] S. Plimpton, Fast parallel algorithms for short-range molecular dynamics, J. Comput. Phys. 117 (1995) 1–19, https://doi.org/10.1006/jcph.1995.1039.
[21] A. Stukowski, Visualization and analysis of atomistic simulation data with OVITO–the Open Visualization Tool, Model. Simulat. Mater. Sci. Eng. 18 (2009), 015012, https://doi.org/10.1088/0965-0393/18/1/015012.
[22] X.W. Zhou, R.A. Johnson, H.N.G. Wadley, Misfit-energy-increasing dislocations in vapor-deposited CoFe/NiFe multilayers, Phys. Rev. B 69 (2014), 144113, https://doi.org/10.1103/PhysRevB.69.144113.
[23] C. Liu, Y. Li, T. Shi, Q. Peng, F. Gao, Oxygen defects stabilize the crystal structure of MgAl2O4 spinel under irradiation, J. Nucl. Mater. 527 (2019), 151830, https://doi.org/10.1016/j.jnucmat.2019.151830.
[24] J. Tian, H. Wang, Q. Feng, J. Zheng, X. Liu, W. Zhou, Heavy radiation damage in alpha zirconium at cryogenic temperature: a computational study, J. Nucl. Mater. 555 (2021), 153159, https://doi.org/10.1016/j.jnucmat.2021.153159.
[25] X.M. Bai, A.F. Voter, R.G. Hoagland, M. Nastasi, B.P. Uberuaga, Efficient annealing of radiation damage near grain boundaries via interstitial emission, Science 327 (2010) 1631–1634, https://doi.org/10.1126/science.1183723.
[26] H. Huang, X. Tang, K. Xie, Q. Peng, Enhanced self-healing of irradiation defects near a Ni–graphene interface by damaged graphene: insights from atomistic modeling, J. Phys. Chem. Solid. 151 (2021), 109909, https://doi.org/10.1016/j.jpcs.2020.109909.
[27] F. Granberg, J. Byggmästar, K. Nordlund, Defect accumulation and evolution during prolonged irradiation of Fe and FeCr alloys, J. Nucl. Mater. 528 (2020), 151843, https://doi.org/10.1016/j.jnucmat.2019.151843.
[28] R. Voskoboinikov, Statistics of primary radiation defects in pure nickel, Nucl. Instrum. Methods B 478 (2020) 201–204, https://doi.org/10.1016/j.nimb.2020.06.034.
[29] S.J. Wooding, D.J. Bacon, W.J. Phythian, A computer simulation study of displacement cascades in α-titanium, Philos. Mag. A 72 (1995) 1261–1279, https://doi.org/10.1080/01418619508236254.
[30] F. Gao, D.J. Bacon, L.M. Howe, C.B. So, Temperature-dependence of defect creation and clustering by displacement cascades in α-zirconium, J. Nucl. Mater. 294 (2001) 288–298, https://doi.org/10.1016/S0022-3115(01)00483-4.
[31] S.J. Zinkle, J.T. Busby, Structural materials for fission & fusion energy, Mater. Today 12 (2009) 12–19, https://doi.org/10.1016/S1369-7021(09)70294-9.
[32] X. Xiao, Fundamental mechanisms for irradiation-hardening and embrittlement: a review, Metals 9 (2019) 1132, https://doi.org/10.3390/met9101132.
[33] H. Yuya, K. Yabuuchi, A. Kimura, Radiation embrittlement of clad-HAZ of RPV of a decommissioned BWR plant, J. Nucl. Mater. 557 (2021), 153300, https://doi.org/10.1016/j.jnucmat.2021.153300.
[34] B.D. Wirth, How does radiation damage materials? Science 318 (2007) 923–924, https://doi.org/10.1126/science.1150394.